

Palladium-Catalyzed Asymmetric Phosphination. Scope, Mechanism, and Origin of Enantioselectivity

Natalia F. Blank,[†] Jillian R. Moncarz,[†] Tim J. Brunker,[†] Corina Scriban,[†]
 Brian J. Anderson,[†] Omar Amir,[†] David S. Glueck,^{*,†} Lev N. Zakharov,[‡]
 James A. Golen,[‡] Christopher D. Incarvito,[§] and Arnold L. Rheingold^{‡,§}

Contribution from the 6128 Burke Laboratory, Department of Chemistry, Dartmouth College, Hanover, New Hampshire, 03755, Department of Chemistry, University of California, San Diego, 9500 Gilman Drive, La Jolla, California, 92093, and Department of Chemistry, University of Delaware, Newark, Delaware, 19716

Received January 17, 2007; E-mail: Glueck@Dartmouth.Edu

Abstract: Asymmetric cross-coupling of aryl iodides (ArI) with secondary arylphosphines (PHMe(Ar')), Ar' = (2,4,6)-R₃C₆H₂; R = *i*-Pr (Is), Me (Mes), Ph (Phes)) in the presence of the base NaOSiMe₃ and a chiral Pd catalyst precursor, such as Pd((*R,R*)-Me-Duphos)(*trans*-stilbene), gave the tertiary phosphines PMe(Ar')(Ar) in enantioenriched form. Sterically demanding secondary phosphine substituents (Ar') and aryl iodides with electron-donating *para* substituents resulted in the highest enantiomeric excess, up to 88%. Phosphination of *ortho*-substituted aryl iodides required a Pd(Et-FerroTANE) catalyst but gave low enantioselectivity. Observations during catalysis and stoichiometric studies of the individual steps suggested a mechanism for the cross-coupling of PhI and PHMe(Is) (**1**) initiated by oxidative addition to Pd(0) yielding Pd((*R,R*)-Me-Duphos)(Ph)(I) (**3**). Reversible displacement of iodide by PHMe(Is) gave the cation [Pd((*R,R*)-Me-Duphos)(Ph)(PHMe(Is))]I (**4**), which was isolated as the triflate salt and crystallographically characterized. Deprotonation of **4-OTf** with NaOSiMe₃ gave the phosphido complex Pd((*R,R*)-Me-Duphos)(Ph)(PMels) (**5**); an equilibrium between its diastereomers was observed by low-temperature NMR spectroscopy. Reductive elimination of **5** yielded different products depending on the conditions. In the absence of a trap, the unstable three-coordinate phosphine complex Pd((*R,R*)-Me-Duphos)(PMels(Ph)) (**6**) was formed. Decomposition of **5** in the presence of PhI gave PMels(Ph) (**2**) and regenerated **3**, while trapping with phosphine **1** during catalysis gave Pd((*R,R*)-Me-Duphos)(PHMe(Is))₂ (**7**), which reacted with PhI to give **3**. Deprotonation of 1:1 or 1.4:1 mixtures of cations **4-OTf** gave the same 6:1 ratio of enantiomers of PMels(Ph) (**2**), suggesting that the rate of P inversion in **5** was greater than or equal to the rate of reductive elimination. Kinetic studies of the first-order reductive elimination of **5** were consistent with a Curtin–Hammett–Winstein–Holness (CHWH) scheme, in which pyramidal inversion at the phosphido ligand was much faster than P–C bond formation. The absolute configuration of the phosphine (*S_P*)-PMels(*p*-MeOC₆H₄) was determined crystallographically; NMR studies and comparison to the stable complex **5-Pt** were consistent with an *R_P*-phosphido ligand in the major diastereomer of the intermediate Pd((*R,R*)-Me-Duphos)(Ph)(PMels) (**5**). Therefore, the favored enantiomer of phosphine **2** appeared to be formed from the major diastereomer of phosphido intermediate **5**, although the minor intermediate diastereomer underwent P–C bond formation about three times more rapidly. The effects of the diphosphine ligand, the phosphido substituents, and the aryl group on the ratio of diastereomers of the phosphido intermediates Pd(diphos*)(Ar)(PMeAr'), their rates of reductive elimination, and the formation of three-coordinate complexes were probed by low-temperature ³¹P NMR spectroscopy; the results were also consistent with the CHWH scheme.

Introduction

Metal-catalyzed asymmetric synthesis depends on chiral ligands, especially phosphines.¹ Chiral phosphines are usually prepared either by resolution or by using a stoichiometric amount of a chiral auxiliary.² Despite the successful application of

asymmetric catalysis to the preparation of other high-value chiral compounds, metal-catalyzed asymmetric syntheses of these ligands are rare.³ However, we and others have recently described new approaches to P-stereogenic chiral phosphines via metal-catalyzed hydrophosphination of alkenes,⁴ Pt- or Ru-catalyzed alkylation of secondary phosphines,⁵ or Pd-catalyzed phosphination of aryl halides.⁶ Better understanding of the scope

[†] Dartmouth College.

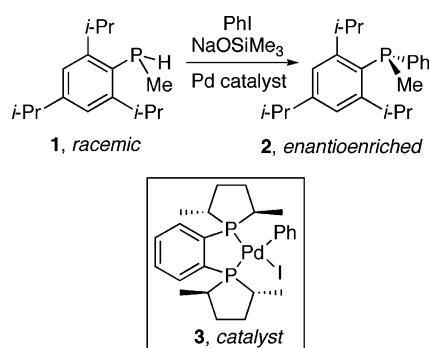
[‡] University of California, San Diego.

[§] University of Delaware.

(1) (a) Noyori, R. *Asymmetric Catalysis in Organic Synthesis*; Wiley-Interscience: New York, 1994. (b) Blaser, H.-U., Schmidt, E., Eds. *Asymmetric Catalysis on Industrial Scale. Challenges, Approaches, and Solutions*; Wiley-VCH: Weinheim, 2004.

(2) (a) Pietrusiewicz, K. M.; Zablocka, M. *Chem. Rev.* **1994**, *94*, 1375–1411. (b) Kagan, H. B.; Sasaki, M. In *The Chemistry of Organophosphorus Compounds*; Hartley, F. R., Ed.; John Wiley and Sons: Chichester, U.K., 1990; Vol. 1, pp 51–102. (c) Tang, W.; Zhang, X. *Chem. Rev.* **2003**, *103*, 3029–3070.

Scheme 1



and limitations of these metal-catalyzed processes, and knowledge of their mechanisms and the origin of enantioselectivity, should help to make asymmetric catalysis a more efficient and practical route to valuable chiral phosphines. With this goal in mind, we report here details of our studies of the Pd-catalyzed asymmetric phosphination of aryl iodides.^{6a}

Results and Discussion

Selection of Catalyst and Substrates for a Test Reaction.

In any catalytic asymmetric phosphine synthesis, the chiral ancillary ligand must resist displacement from the metal by the excess phosphine substrate and products. Therefore, we used the rigid bidentate chiral alkylphosphine (*R,R*)-Me-Duphos to ensure tight binding to the metal.⁷ The secondary phosphine PHMe(Is) (**1**, Is = 2,4,6-(*i*-Pr)₃C₆H₂), with a large Is and a small Me substituent, was selected in hopes of maximizing steric differentiation at P in the diastereomeric intermediates and transition states.⁸ The base NaOSiMe₃ was chosen to minimize the concentration of the free phosphido anion [PMeIs][−], which might reduce the Pd catalyst or undergo other side reactions. These design elements were successful; the reaction in Scheme 1 occurred quickly at room temperature (about 1 h with 5 mol % catalyst loading) in high yield and ~70% ee.^{6a}

Table 1. Pd((*R,R*)-Me-Duphos)-Catalyzed Asymmetric Phosphination of PhI with PHMe(Is): Effect of Solvents, Temperature, and Base on Yield and Enantioselectivity^a

entry	equiv of PhI	catalyst loading (mol%)	equiv of base	solvent	T (°C)	yield (%)	ee ^b (%)
1	2	5	1	toluene	22	71 ^c	73
2	1.05	3	1	toluene	22	93 ^d	72
3	1.07	2.5	1	toluene	22	88 ^d	73
4	1.1	5	1	pentane	22	90 ^d	78
5	2	7	1	THF	22	69 ^c	66
6	2	7	1	MeCN	22	60 ^c	58
7	1.1	5	1	DMSO	22	78 ^c	55
8	1	5	1	toluene	4	82 ^c	82
9	2	5	1	toluene	50	60 ^d	42
10 ^e	1.05	5	1	toluene	22	91 ^d	70
11 ^f	1.1	2.5	2	toluene	22	90 ^d	73
12 ^f	1.1	2.5	3	toluene	22	89 ^d	75
13 ^f	1.1	2.5	10	toluene	22	96 ^d	74
14 ^g	1.1	2.5	1	toluene	22	83 ^d	75

^a The catalyst precursor was Pd((*R,R*)-Me-Duphos)(Ph)(I), and the base was NaOSiMe₃ (1.0 M in THF). ^b The phosphine was complexed with Pd((*S*)-Me₂NCH(Me)C₆H₄)(μ-Cl)₂ in C₆D₆; integration of CHMe signals in the ¹H NMR spectrum gave the de, which corresponds to the phosphine ee (see the Supporting Information for details). ^c NMR yield, from integration of the ¹H NMR spectrum after addition of Pd((*S*)-Me₂NCH(Me)C₆H₄)(μ-Cl)₂ to the phosphine product isolated after column chromatography on silica gel. ^d Isolated yield after column chromatography. ^e Scale: 500 mg of PHMe(Is). ^f Catalyst precursor: Pd((*R,R*)-Me-Duphos)(*trans*-stilbene). ^g Base = NaN(SiMe₃)₂.

Effect of Reaction Conditions. Table 1 shows the effect of reaction conditions on the rate and selectivity of this test cross-coupling. An excess of PhI was not required, which simplified the workup (entries 1 and 2). The ee decreased slightly with increased solvent polarity (entries 3–7), so the preferred solvent was toluene or pentane. The catalyst loading could be decreased to 2.5 mol % without any loss of enantioselectivity (entry 3). Enantioselectivity increased at low temperature and decreased on heating the reaction mixture (compare entries 1, 8, and 9). Entries 10–14 showed that only 1 equiv of base was required; using excess NaOSiMe₃ or changing the base to NaN(SiMe₃)₂, however, had little effect on yield and ee. In general, the reaction appeared to be quantitative, and isolated yields were limited by losses during chromatographic workup.

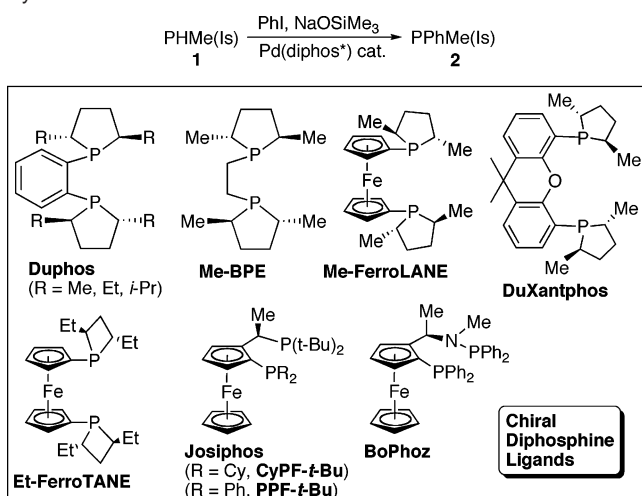
Screening of reaction conditions was done on a small scale (20–25 mg of secondary phosphine **1**). On a larger scale, isolation of air-sensitive **2** by chromatography under nitrogen was inconvenient, but a modified workup (entry 10) avoided this problem. Coupling of 500 mg of PHMe(Is) (2 mmol) with PhI using 5 mol % of Pd((*R,R*)-Me-Duphos)(Ph)(I) (**3**) was complete in 2 h. After solvent was removed, extraction with petroleum ether and filtration through a short pad of silica followed by washing the silica with petroleum ether/THF (9:1) eluent reproducibly gave the product phosphine in 90% yield and 70% ee.

Catalyst Screening. Several chiral Pd(diphos*)(Ph)(I) and Pd(diphos*)(*trans*-stilbene) complexes were screened as catalyst precursors in the reaction of Scheme 1 (Scheme 2, Table 2).⁹

The yields and ee of the product phosphine depended strongly on the nature of the chiral diphos* ligand. We first investigated bis(phospholanes) structurally analogous to Me-Duphos. Either the original catalyst Pd((*R,R*)-Me-Duphos)(Ph)(I) (**3**) or the Pd-

- (3) (a) Burk, M. J.; Feaster, J. E.; Nugent, W. A.; Harlow, R. L. *J. Am. Chem. Soc.* **1993**, *115*, 10125–10138. (b) Hoge, G. *J. Am. Chem. Soc.* **2003**, *125*, 10219–10227. (c) Shimizu, H.; Saito, T.; Kumabayashi, H. *Adv. Synth. Catal.* **2003**, *345*, 185–189. (d) Marinetti, A.; Genet, J.-P. *C. R. Chimie* **2003**, *6*, 507–514.
- (4) (a) Kovacic, I.; Wicht, D. K.; Grewal, N. S.; Glueck, D. S.; Incarvito, C. D.; Guzei, I. A.; Rheingold, A. L. *Organometallics* **2000**, *19*, 950–953. (b) Douglass, M. R.; Ogasawara, M.; Hong, S.; Metz, M. V.; Marks, T. J. *Organometallics* **2002**, *21*, 283–292. (c) Sadow, A. D.; Haller, I.; Fadini, L.; Togni, A. *J. Am. Chem. Soc.* **2004**, *126*, 14704–14705. (d) Sadow, A. D.; Togni, A. *J. Am. Chem. Soc.* **2005**, *127*, 17012–17024. (e) Scriban, C.; Kovacic, I.; Glueck, D. S. *Organometallics* **2005**, *24*, 4871–4874. (f) Kovacic, I.; Scriban, C.; Glueck, D. S. *Organometallics* **2006**, *25*, 536–539. (g) Scriban, C.; Glueck, D. S.; Zakharov, L. N.; Kassel, W. S.; DiPasquale, A. G.; Golen, J. A.; Rheingold, A. L. *Organometallics* **2006**, *25*, 5757–5767. For related reactions involving metal-catalyzed enantioselective addition of P–H bonds to unsaturated substrates, see: (h) Shulyupin, M. O.; Franciu, G.; Beletskaya, I. P.; Leitner, W. *Adv. Synth. Catal.* **2005**, *347*, 667–672. (i) Xu, Q.; Han, L.-B. *Org. Lett.* **2006**, *8*, 2099–2101. (j) Join, B.; Mimeau, D.; Delacroix, O.; Gaumont, A.-C. *Chem. Commun.* **2006**, 3249–3251.
- (5) (a) Scriban, C.; Glueck, D. S. *J. Am. Chem. Soc.* **2006**, *128*, 2788–2789. (b) Chan, V. S.; Stewart, I. C.; Bergman, R. G.; Toste, F. D. *J. Am. Chem. Soc.* **2006**, *128*, 2786–2787.
- (6) (a) Moncarz, J. R.; Laritcheva, N. F.; Glueck, D. S. *J. Am. Chem. Soc.* **2002**, *124*, 13356–13357. (b) Moncarz, J. R.; Brunner, T. J.; Jewett, J. C.; Orchowski, M.; Glueck, D. S.; Sommer, R. D.; Lam, K.-C.; Incarvito, C. D.; Concolino, T. E.; Ceccarelli, C.; Zakharov, L. N.; Rheingold, A. L. *Organometallics* **2003**, *22*, 3205–3221. (c) Korff, C.; Helmchen, G. *Chem. Commun.* **2004**, 530–531. (d) Pican, S.; Gaumont, A.-C. *Chem. Commun.* **2005**, 2393–2395.
- (7) Drago, D.; Pregosin, P. S. *Organometallics* **2002**, *21*, 1208–1215.
- (8) Brauer, D. J.; Bitterer, F.; Dorrenbach, F.; Hessler, G.; Stelzer, O.; Kruger, C.; Lutz, F. Z. *Naturforsch. B* **1996**, *51*, 1183–1196.

- (9) Brunner, T. J.; Blank, N. F.; Moncarz, J. R.; Scriban, C.; Anderson, B. J.; Glueck, D. S.; Zakharov, L. N.; Golen, J. A.; Sommer, R. D.; Incarvito, C. D.; Rheingold, A. L. *Organometallics* **2005**, *24*, 2730–2746.

Scheme 2. Chiral Diphosphine Ligands Screened in Pd-Catalyzed Synthesis of **2** from **1****Table 2.** Pd(diphos*)-Catalyzed Asymmetric Synthesis of PPhMe(Is) (**2**) from PHMe(Is) (**1**)^a

entry	Diphos*	precursor	solvent	t (h)	yield (%)	ee ^b (%)
1 ^c	(<i>R,R</i>)-Me-Duphos	B	toluene	1	71 ^d	73
2	(<i>R,R</i>)-Me-Duphos	A	toluene	1	97 ^e	76
3	(<i>R,R</i>)-Et-Duphos	B	toluene	1	63 ^d	72
4	(<i>R,R</i>)- <i>i</i> -Pr-Duphos	B	toluene	16	83 ^e	73
5	(<i>R,R</i>)- <i>i</i> -Pr-Duphos	A	toluene	16	98 ^e	71
6	(<i>R,R</i>)-Me-BPE	B	THF	20	100 ^e	−18 ^f
7	(<i>S,S</i>)-Me-FerroLANE	B	toluene	4	89 ^e	28
8 ^g	(<i>S,S</i>)-Et-FerroTANE	B	THF	24	nd ^h	−45 ^f
9 ⁱ	(<i>S,S</i>)-Et-FerroTANE	B	THF	48	nd ^h	−50 ^f
10	(<i>S,S</i>)-Et-FerroTANE	B	toluene	24	96 ^e	−37 ^f
11 ^j	(<i>R,S</i>)-PPF- <i>t</i> -Bu	B	THF	72	nd ^h	−21 ^f
12	(<i>R,S</i>)-PPF- <i>t</i> -Bu	A	toluene	48	94	3
13	(<i>R,S</i>)-CyPF- <i>t</i> -Bu	A	toluene	48 ^k	72	rac
14	(<i>R,S</i>)-BoPhoz	A	toluene	24 ^k	72	rac

^a The standard procedure used 5 mol % of the catalyst precursors Pd(diphos*)(*trans*-stilbene) (A) or Pd(diphos*)(Ph)(I) (B), PHMe(Is), PhI (1.05–1.1 equiv), and NaOSiMe₃ (1.0 M in THF, 1 equiv) at room temperature, except where noted. ^b The phosphine was complexed with Pd(((*S*)-Me₂NCH(Me)C₆H₄)(μ-Cl))₂ in C₆D₆; integration of CHMe signals in the ¹H NMR spectrum gave the de which corresponds to the phosphine ee. ^c 2 equiv of PhI (Table 1, entry 1). ^d From integration of the ¹H NMR spectrum after addition of Pd(((*S*)-Me₂NCH(Me)C₆H₄)(μ-Cl))₂ to the phosphine product isolated after column chromatography on silica gel. ^e Isolated yield after column chromatography. ^f This catalyst selectively gave the opposite enantiomer of the phosphine. ^g 10 mol % catalyst precursor, 2 equiv of PhI. ^h nd = not determined. ⁱ 10 mol % of the catalyst precursor was added to AgOTf and filtered into a solution of **1**, PhOTf (2 equiv), and NEt(*i*-Pr)₂. ^j The catalyst precursor was the cation [Pd(PPF-*t*-Bu)(Ph)(NCMe)]⁺[OTf][−] (prepared *in situ* from the iodo complex and AgOTf in MeCN; see the Supporting Information), 2 equiv of PhOTf, base = NEt(*i*-Pr)₂. ^k At 50 °C.

(0) precursor Pd((*R,R*)-Me-Duphos)(*trans*-stilbene) could be used, without significant differences (entries 1 and 2 and entries 4 and 5 for the *i*-Pr-Duphos analogue). The change from Me- to Et-Duphos had little effect (entries 1–3), and results with (*R,R*)-*i*-Pr-Duphos were similar (entries 4 and 5). This was surprising; the Cahn–Ingold–Prelog priority rules mean that (*R,R*)-Me- and *i*-Pr-Duphos have opposite absolute configurations and might be expected to preferentially yield opposite enantiomers of the product.^{3a} NMR and structural data for the catalyst precursors⁹ indicated that these results were not a consequence of mislabeling of the ligand stereochemistry; possible mechanistic explanations for the reversal of enantioselectivity are discussed in more detail below.¹⁰

Table 3. Pd((*R,R*)-Me-Duphos)-Catalyzed Coupling of Secondary Methylarylphosphines with Aryl Halides^a

entry	phosphine	ArX	time (h)	yield ^b (%)	ee ^c (%)	σ _p ^d
1 ^e	PHMe(Is)	PhBr	1	53	38	
2 ^f	PHMe(Is)	PhOTf	1	70	50	
3	PHMe(Is)	PhI	1	97	76	0
4	PHMe(Is)	<i>p</i> -PhOC ₆ H ₄ I	1	89	88 ^g	−0.32
5	PHMe(Is)	<i>p</i> -MeOC ₆ H ₄ I	6	96	82	−0.27
6	PHMe(Is)	<i>p</i> -NH ₂ C ₆ H ₄ I	1	88	79 ^g	−0.66
7	PHMe(Is)	<i>p</i> -MeC ₆ H ₄ I	22	98	78	−0.17
8	PHMe(Is)	<i>p</i> -CF ₃ C ₆ H ₄ I	2	96	45	0.54
9	PHMe(Is)	<i>p</i> -IC ₆ H ₄ I	2	68	40	0.18
10 ^h	PHMe(Is)	<i>p</i> -NO ₂ C ₆ H ₄ I	1	73	12	0.78
11 ⁱ	PHMe(Is)	<i>p</i> -IC ₆ H ₄ I	2	91	33 ^j	
12	PHMe(Is)	8-QuinolylI	6	75	27 ^k	
13	PHMe(Is)	3,5-Me ₂ C ₆ H ₃ I	456	93	15	
14	PHMe(Is)	<i>o</i> -C ₅ H ₄ NI	6	98	12	
15	PHMe(Is)	1-NaphI	5	98	nd ^l	
16	PHMe(Mes)	PhI	4	59	56	0
17	PHMe(Mes)	<i>p</i> -MeOC ₆ H ₄ I	48	90	48 ^g	−0.27
18	PHMe(Mes)	<i>p</i> -CF ₃ C ₆ H ₄ I	48	75	7 ^g	0.54
19	PHMe(Phes)	PhI	24	91	−59 ^m	0
20	PHMe(Phes)	<i>p</i> -MeOC ₆ H ₄ I	1	81	−65 ^{g,m}	−0.27
21	PHMe(Phes)	<i>p</i> -PhOC ₆ H ₄ I	24	84	−82 ^m	−0.32
22 ⁿ	PHMe(Men)	PhI	48	68	73	
23 ^{n,o}	PHMe(Men)	PhI	48	72	91	

^a The catalyst precursor was 5 mol % of Pd((*R,R*)-Me-Duphos)(*trans*-stilbene). Reactions used 0.1 mmol of PHMe(Ar'), 1.05–1.1 equiv of ArX, and NaOSiMe₃ (1.0 M in THF, 1 equiv) at room temperature in toluene, unless otherwise stated. Mes = 2,4,6-Me₃C₆H₂, Phes = 2,4,6-Ph₃C₆H₂. See Experimental Section for details. ^b Isolated yield after column chromatography. ^c The phosphine was complexed with Pd(((*S*)-Me₂NCH(Me)C₆H₄)(μ-Cl))₂ in C₆D₆; integration of CHMe signals in the ¹H NMR spectrum gave the de which corresponds to the phosphine ee. ^d Hammett substituent constant. ^e Catalyst precursor: Pd((*R,R*)-Me-Duphos)(Ph)(I), 2 equiv of PhBr, 50 °C. ^f Catalyst precursor: Pd((*R,R*)-Me-Duphos)(Ph)(I), 2 equiv of PhOTf. ^g The phosphine was complexed with Pd(((*S*)-Me₂NCH(Me)C₆H₄)(μ-Cl))₂ in C₆D₆; integration of P signals in the ³¹P NMR spectrum gave the de which corresponds to the phosphine ee. ^h Catalyst precursor: Pd((*R,R*)-Me-Duphos)(*p*-NO₂C₆H₄)(I) (see below). ⁱ 2 equiv of NaOSiMe₃, 2 equiv of PHMe(Is). ^j de = diastereomeric excess. ^k ee was determined for the [(N-C*)Pd(P-N)]⁺[OTf][−] adduct formed in reaction of (N-C*)Pd(Cl)(P(8-Quinolyl)Me(Is)) with AgOTf. ^l ¹H NMR signals of the (N-C*)Pd(P(1-Naph)Me(Is)) complex were very broad, so ee was not determined (nd). ^m The negative sign indicates that the ³¹P and ¹H NMR chemical shift trends for Pd adducts of these phosphine products were the opposite of those observed for PArMe(Is) and PArMe(Mes) (Supporting Information). ⁿ From ref 14. Men = (−)-menthyl; here, the de is reported. ^o Catalyst precursor = Pd((*R,R*)-*i*-Pr-Duphos)(*trans*-stilbene).

Several Ni(Me-Duphos) catalyst precursors (see the Supporting Information) were inferior to the Pd analogue; reaction did not go to completion, and several byproducts were formed. With Pd, the Me-BPE ligand, less rigid than Duphos, gave reduced ee (entry 6), while the ferrocene-based bis(phospholane) Me-FerroLANE (entry 7) was also inferior. Catalysis with the wide-bite-angle DuXantphos ligand was very slow, and byproducts formed. Despite promising results for asymmetric phosphination of secondary diarylphosphines with (*S,S*)-Et-FerroTANE reported recently by Korff and Helmchen,^{6c} this ligand was less enantioselective in the test reaction (entries 8–10). It did enable use of PhOTf with a Pd(II) precursor (entry 9; see also entry 11 for related results with PPF-*t*-Bu and Table 3, entry 2 for use of PhOTf with a Pd(Me-Duphos) catalyst). Stilbene complexes of the Josiphos derivatives PPF-*t*-Bu and CyPF-*t*-Bu or the related ferrocenylphosphine BoPhoz (entries 12–14)

(10) For other examples of reversal of enantioselectivity in asymmetric catalysis, see: (a) Evans, D. A.; Johnson, J. S.; Burgey, C. S.; Campos, K. R. *Tetrahedron Lett.* **1999**, 40, 2879–2882. (b) Sibi, M. P.; Liu, M. *Curr. Org. Chem.* **2001**, 5, 719–755. (c) Zanoni, G.; Castronovo, F.; Franzini, M.; Vidari, G.; Giannini, E. *Chem. Soc. Rev.* **2003**, 32, 115–129.

Scheme 3. Substrate Scope in Pd-Catalyzed Asymmetric Phosphination ($R = i\text{-Pr, Me, Ph}$; for Ar Groups See Tables 3 and 4)

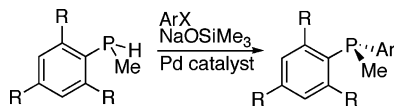


Table 4. Pd((*S,S*)-Et-FerroTANE)-catalyzed Coupling of PHMe(Is) with *o*-Substituted Aryl Iodides and Organometallic Iodocyclopentadienyl Complexes^a

entry	iodo substrate	time (h)	yield ^b (%)	ee ^c (%)
1	<i>o</i> -MeOC ₆ H ₄ I	1	51	racemic
2	<i>o</i> -CNC ₆ H ₄ I	42	83	3
3	<i>o</i> -MeC ₆ H ₄ I	9	88	nd ^d
4 ^e	FcI	6	100	8
5 ^f	CymI	6	82	5

^a The catalyst precursor was Pd((*S,S*)-Et-FerroTANE)(*trans*-stilbene) (5 mol %). Reactions were done with 1 equiv of ArI and 1 equiv of NaOSiMe₃ (1.0 M in THF) in toluene at room temperature. See Experimental Section for details. ^b Isolated yield after column chromatography on silica. ^c The phosphine was complexed with (Pd((*S,S*)-Me₂NCH(Me)C₆H₄)(μ-Cl))₂ in C₆D₆; integration of the ³¹P NMR spectrum gave the de which corresponds to the phosphine ee. ^d nd = not determined; the ³¹P NMR signals overlapped, and suitable ¹H NMR signals could not be identified (see Supporting Information). ^e Fc = ferrocenyl, C₅H₄FeC₅H₅, 70 °C. ^f Cym = cymantrenyl, C₅H₄Mn(CO)₃, 50 °C.

gave slow turnover and no enantioselectivity; for the latter two, ligand displacement during catalysis was observed.

Substrate Scope. Since screening of the test reaction of Schemes 1 and 2 revealed that the original Me-Duphos ligand gave the highest enantioselectivity, we used it to explore the scope of the reaction. Coupling of three secondary phosphines PHMe(Ar') (Ar' = 2,4,6-R₃C₆H₂, R = *i*-Pr (Is), Me (Mes), or Ph (Phes)) with aryl iodides ArI gave enantioenriched methyl-diarylphosphines PMe(Ar')(Ar) in high yields (Scheme 3, Tables 3 and 4). The racemic phosphines were prepared for comparison using the catalyst precursor Pd(P(*o*-Tol)₃)₂Cl₂ and characterized spectroscopically, by elemental analyses and mass spectroscopy, and, in several cases, by X-ray crystallography (Supporting Information).

Entries 1–3 in Table 3 showed that phenyl bromide (at 50 °C) and phenyl triflate could also be used, but selectivity was lower than that with PhI. Therefore, we studied exclusively aryl iodides.¹¹ The disubstituted *p*-diiodobenzene could be selectively coupled with 1 or 2 equiv of PHMe(Is) (entries 9 and 11). The Pd(Me-Duphos) catalyst tolerated other aryl iodides with *p*- or *m*-substituents (Table 3). Double *m*-substitution appeared to slow the reaction for 3,5-Me₂C₆H₃I (entry 13), and no turnover was observed for the analogous substrate 3,5-(CF₃)₂C₆H₃I. Although coupling of *o*-iodopyridine was fast (entry 14) and *o*-MeC₆H₄I also reacted smoothly, catalytic turnover was very slow with other *o*-substituted substrates (*o*-MeOC₆H₄I, *o*-ClC₆H₄I) or did not occur (MesI, Mes = 2,4,6-Me₃C₆H₂).

A Pd(Et-FerroTANE) catalyst promoted the coupling of *o*-substituted aryl iodides, as well as iron and manganese iodocyclopentadienyl complexes, but in disappointingly low ee (Table 4). This poor selectivity did not appear to result exclusively from catalyst decomposition, since some Pd intermediates were observed during catalysis (Supporting Information).

For the Pd(Me-Duphos) catalyst, while yields were generally high and reactions were fast, with a few exceptions, such as

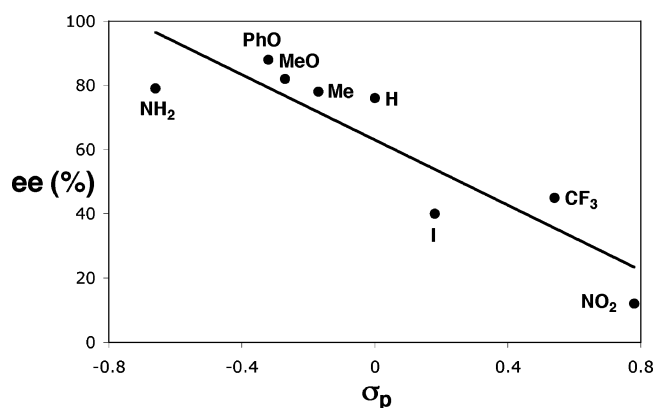


Figure 1. Correlation between ee of the phosphines P(*p*-XC₆H₄)Me(Is) and the substituent constant σ_p (Hammett plot).¹²

entry 13, ee depended strongly on the substrate. This was particularly evident from results with *p*-substituted aryl iodides, where steric effects are presumably minimal. More electron-donating *p*-substituents resulted in higher ee (see entries 3–10 with PHMe(Is)). A Hammett plot of product ee vs substituent constants σ_p , which are listed in Table 3,¹² gave a reasonable correlation (Figure 1). The same trend was observed for the other secondary phosphine substrates (Table 3, entries 16–21). However, an attempt to exploit these observations in the coupling of PHMe(Is) with *p*-Me₂NC₆H₄I ($\sigma_p = -0.83$)¹² led to immediate catalyst decomposition and formation of Pd((*R,R*)-Me-Duphos)₂.^{6b}

While varying the aryl iodide with a given secondary phosphine substrate revealed the electronic effects of *p*-substitution, measuring the ee for one aryl iodide with different secondary phosphines showed the effect of phosphine structure on enantioselectivity (see Table 3, entries 3, 16, and 19 (PhI); 5, 17, and 20 (*p*-MeOC₆H₄I); 8 and 18 (*p*-CF₃C₆H₄I); and 4 and 21 (*p*-PhOC₆H₄I)). In particular, enantiomeric excesses were similar for PHMe(Is) and PHMe(Phes) but lower for PHMe(Mes), perhaps because Is and Phes are comparable in size and both larger than Mes. Catalyst turnover did not occur with the even bulkier PHMe(Mes*) (Mes* = 2,4,6-(*t*-Bu)₃C₆H₂).^{8,13} We have reported elsewhere the diastereoselective coupling of the secondary *dialkyl*phosphine PHMe(Men) (Men = (–)-menthyl) with PhI (entries 22 and 23), but catalyst decomposition occurred during the reaction and Pd((*R,R*)-Me-Duphos)₂ formed.¹⁴

The enantiomeric excess of the new phosphines was determined by integration of the NMR spectra of their diastereomeric adducts with the chiral Pd fragment Pd((*S,S*)-Me₂NCH(Me)C₆H₄)-(Cl).¹⁵ In this assay, the adducts of PMe(Ar')(Ar) showed similar features for Ar' = Is and Mes; the ³¹P NMR signals for the minor diastereomer usually appeared at lower field than those for the major one, and in the ¹H NMR spectra they appeared in the opposite order (Supporting Information Table S2). These trends suggested that the Pd((*R,R*)-Me-Duphos) catalyst consistently favored one hand of the phosphine product. The order of NMR shifts was reversed for PArMe(Phes). To reflect this difference, ee values in entries 19–21 of Table 3 are arbitrarily

(11) For Pd-catalyzed phosphination using aryl bromides and chlorides, see: Murata, M.; Buchwald, S. L. *Tetrahedron* **2004**, *60*, 7397–7403.

(12) (a) Hansch, C.; Leo, A.; Taft, R. W. *Chem. Rev.* **1991**, *91*, 165–195. (b) McDaniel, D. H.; Brown, H. C. *J. Org. Chem.* **1958**, *23*, 420–427.
(13) Yoshifuji, M.; Shibayama, K.; Inamoto, N. *Chem. Lett.* **1984**, 115–118.
(14) Blank, N. F.; McBroom, K. C.; Glueck, D. S.; Kassel, W. S.; Rheingold, A. L. *Organometallics* **2006**, *25*, 1742–1748.
(15) Kyba, E. P.; Rines, S. P. *J. Org. Chem.* **1982**, *47*, 4800–4801.

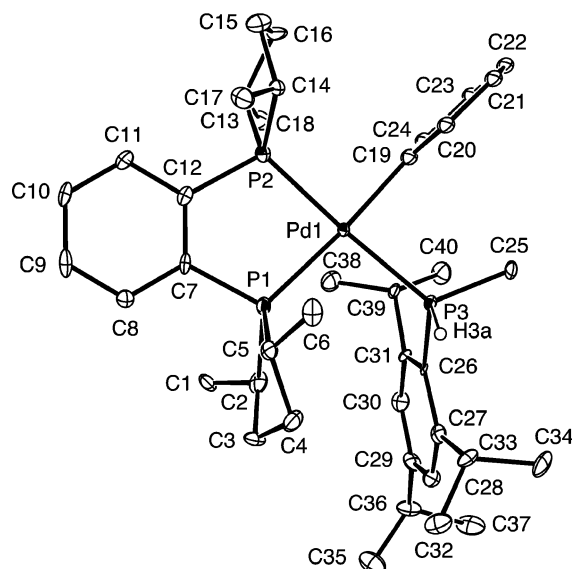
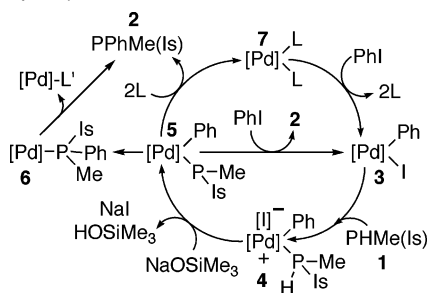


Figure 2. ORTEP diagram of $[\text{Pd}((R,R)\text{-Me-Duphos})(\text{Ph})(\text{PHMeIs})][\text{OTf}] \cdot 2\text{THF}$ (the anion and solvent molecules were omitted, and only the P–H hydrogen is shown).

Scheme 4. Proposed Mechanism for Pd-Catalyzed Synthesis of **2** from **1** ($[\text{Pd}] = \text{Pd}((R,R)\text{-Me-Duphos})$, $\text{L} = \text{PHMe(Is)}$ (**1**), $\text{L}' = (R,R)\text{-Me-Duphos}$)



listed with a minus sign; note that we have determined the absolute configuration of only one phosphine product (see below).

Mechanism of Pd-Catalyzed Asymmetric Phosphination (Scheme 4). Study of the individual steps in a potential mechanism for the $\text{Pd}((R,R)\text{-Me-Duphos})$ -catalyzed coupling of PHMe(Is) with PhI (Scheme 4) provided information on the mechanism of P–C bond formation. Treatment of $\text{Pd}((R,R)\text{-Me-Duphos})(\text{Ph})(\text{I})$ (**3**) with PHMe(Is) (**1**) led to broadening of the ^{31}P NMR peaks of the phosphine at room temperature. Low-temperature ^{31}P NMR spectroscopy showed that the phosphine reversibly displaced iodide to form the cation $[\text{Pd}((R,R)\text{-Me-Duphos})(\text{Ph})(\text{PHMe(Is)})][\text{I}]$ (**4**) as a mixture of diastereomers; the equilibrium favored neutral **3**. Cation **4** was independently synthesized as the isolable triflate salt (**4-OTf**) from **3**, phosphine **1**, and AgOTf .¹⁶ Using a stoichiometric amount of PHMe(Is) gave a 1:1 mixture of diastereomers of **4-OTf**. Heating this material in THF, or use of excess phosphine in the original synthesis, gave **4-OTf** in 1:1.4 ratio.

As expected, the crystal structure of **4-OTf** (Figure 2, Table 5 and the Supporting Information) was very similar to that of the Pt analogue; in both cases the crystal examined contained the R_P -diastereomer.¹⁶ While two of the three Pd–P bonds were

Table 5. Selected Bond Lengths (Å) and Angles (deg) for the Cations $[\text{M}((R,R)\text{-Me-Duphos})(\text{Ph})(\text{PHMeIs})]^+$ ($\text{M} = \text{Pd}$ or Pt)^a

bond/angle	M = Pd	M = Pt
M–P1	2.3204(19)	2.3096(11)
M–P2	2.2775(19)	2.2772(13)
M–P3	2.3347(18)	2.3126(13)
M–C	2.054(7)	2.082(4)
C–M–P2	89.82(18)	90.21(13)
C–M–P1	173.4(2)	172.02(16)
P2–M–P1	85.53(7)	85.52(4)
C–M–P3	87.7(2)	87.26(13)
P2–M–P3	174.48(7)	177.11(4)
P1–M–P3	96.53(6)	96.82(4)
C(Me)–P3–C(Is)	104.3(3)	103.9(3)
C(Me)–P3–M	118.2(2)	118.19(19)
C(Is)–P3–M	118.6(2)	120.38(15)

^a Pd complex **4** (anion = OTf) crystallized with 2 equiv of THF. The Pt complex (anion = BF_4) crystallized with 1 equiv of CH_2Cl_2 .¹⁶

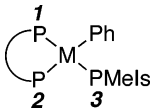
slightly longer than the Pt–P ones, the Pd–C(Ph) distance was shorter than the Pt–C one. Similar observations in simpler compounds have been rationalized on the basis of hard–soft considerations and relativistic effects.¹⁷

Treatment of **3** with PHMe(Is) and NaOSiMe_3 at low temperature gave the phosphido complex $\text{Pd}((R,R)\text{-Me-Duphos})(\text{Ph})(\text{PMeIs})$ (**5**, Scheme 4). We considered several possible mechanisms for this reaction. In analogous Pt chemistry, reaction of $\text{Pt}((R,R)\text{-Me-Duphos})(\text{Ph})(\text{X})$ ($\text{X} = \text{Cl}$ or Br) with NaOSiMe_3 gave the silanolate complex $\text{Pt}((R,R)\text{-Me-Duphos})(\text{Ph})(\text{OSiMe}_3)$, which reacted quickly with PHMe(Is) to give **5-Pt**.^{5a,18} However, the palladium iodide **3** did not react with NaOSiMe_3 . Alternatively, the anion $[\text{PMeIs}]^-$, formed by deprotonation of PHMe(Is) with NaOSiMe_3 , might displace iodide from **3** to give **5**, but **1** and NaOSiMe_3 did not react. We cannot rule out the possibility that such pathways operate via unfavorable equilibria, but cation **4-OTf** reacted quickly with NaOSiMe_3 to give **5**, which suggests that Pd-phosphido formation occurred by coordination followed by deprotonation (Scheme 4).

Phosphido complex **5** was characterized by low-temperature multinuclear NMR spectroscopy (see Table 6 for ^{31}P NMR data and the Supporting Information). Two diastereomers which differ in the absolute configuration of the pyramidal phosphido ligand would be expected,¹⁹ but we observed four diastereomers of the Pt analogue **5-Pt**.¹⁶ The “extra” isomers appeared to be conformational isomers resulting from restricted rotation in the bulky Pt– PMeIs group. Similarly, three diastereomers of **5** were observed (-50°C , 92:2:0.4 ratio, Table 6). Since, unlike **5-Pt**, thermally sensitive **5** could not be purified (see below), it was difficult to rule out the possibility that minor signals in the spectra of **5** were due to impurities. Indeed, independent generation of the iodo complex $\text{Pd}((R,R)\text{-Me-Duphos})(\text{I})(\text{PMeIs})$ showed that it was present in some cases, presumably arising

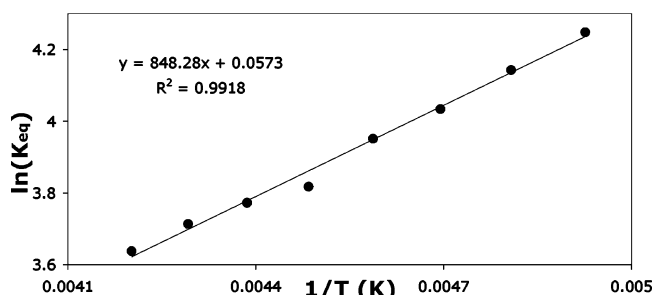
(16) For the analogous Pt complexes, see: (a) ref 5a (b) Scriban, C.; Glueck, D. S.; DiPasquale, A. G.; Rheingold, A. L. *Organometallics* **2006**, *25*, 5435–5448.

(17) (a) Wisner, J. M.; Bartczak, T. J.; Ibers, J. A.; Low, J. J.; Goddard, W. A., III. *J. Am. Chem. Soc.* **1986**, *108*, 347–348. (b) Wisner, J. M.; Bartczak, T. J.; Ibers, J. A. *Organometallics* **1986**, *5*, 2044–2050. (c) Oberhauser, W.; Stampfl, T.; Bachmann, C.; Haid, R.; Langes, C.; Kopacka, H.; Ongania, K.-H.; Bruggeller, P. *Polyhedron* **2000**, *19*, 913–923.
(18) Scriban, C.; Glueck, D. S.; Golen, J. A.; Rheingold, A. L. *Organometallics* **2007**, *26*, 1788–1800.
(19) (a) Wicht, D. K.; Glueck, D. S.; Liable-Sands, L. M.; Rheingold, A. L. *Organometallics* **1999**, *18*, 5130–5140. (b) Wicht, D. K.; Kovacic, I.; Glueck, D. S.; Liable-Sands, L. M.; Incarvito, C. D.; Rheingold, A. L. *Organometallics* **1999**, *18*, 5141–5151. (c) Zhuravel, M. A.; Glueck, D. S.; Zakharov, L. N.; Rheingold, A. L. *Organometallics* **2002**, *21*, 3208–3214.

Table 6. ^{31}P NMR Data for the Phosphido Complexes $\text{M}((R,R)\text{-Me-Duphos})(\text{Ph})(\text{PMels})$ ($\text{M} = \text{Pd}, \text{Pt}$)^a


complex	<i>T</i> (°C)	$\delta(\text{P}_1)$ ($J_{\text{P1-P}}$)	$\delta(\text{P}_2)$ ($J_{\text{P2-P}}$)	$\delta(\text{P}_3)$ ($J_{\text{P3-P}}$)	J_{12}	J_{13}	J_{23}	dr ^b
$\text{Pd}(\text{Me-Duphos})(\text{Ph})$ - (PMels) (5a)	−50	49.0	55.0	−34.0	27	127	13	92
5b		50.1		−22.2	27	137		2
5c				−29.8		130		0.4
$\text{Pt}(\text{Me-Duphos})(\text{Ph})$ - (PMels) (5a-Pt)	−75	56.5 (1653)	57.3 (1868)	−55.9 (889)		136		98
5b-Pt				−47.3 (~940)		136		2.2
5c-Pt				−49.5		142		1.2
5d-Pt				−51.6		134		1

^a All Duphos ligands have (*R,R*) configuration. Chemical shifts in ppm (85% H_3PO_4 external standard). Coupling constants in Hz. Solvent = THF-*d*₈. For atom labeling, see the figure above. In several cases (especially for minor diastereomers), it was not possible to assign Duphos P resonances, so they are omitted. Data for the Pt complex is from ref 16. ^bdr = diastereomer ratio, from integration of the ^{31}P NMR spectra at −50 °C.

**Figure 3.** Temperature dependence of the equilibrium between diastereomers **5a** and **5b** of $\text{Pd}((R,R)\text{-Me-Duphos})(\text{Ph})(\text{PMels})$ in THF/THF-*d*₈. K_{eq} values are the average of two separate measurements (Supporting Information).

from $\text{Pd}((R,R)\text{-Me-Duphos})\text{I}_2$ as an impurity in **3**.²⁰ On warming, peaks due to minor isomer **5c** disappeared and those of **5b** broadened considerably; this behavior may correspond to a coalescence of rotamers as in analogous Pt complexes.¹⁶ We could not observe the expected coalescence of the **5a/5b** signals because of rapid decomposition on warming (see below).

The temperature dependence of the equilibrium between diastereomers **5a** and **5b** from −70 to −35 °C is shown in Figure 3. As desired (see the Introduction), the equilibrium lay far to one side ($K_{\text{eq}} = 70$ at −70 °C in THF/THF-*d*₈). Extrapolation to catalytic conditions at room temperature (298 K) gave $K_{\text{eq}} = 18$ and $\Delta G^\circ_{298} = 1.7$ kcal/mol.

Decomposition of **5** via reductive elimination on warming gave, in the absence of a trap, a mixture of diastereomers of the three-coordinate phosphine complex $\text{Pd}((R,R)\text{-Me-Duphos})\text{(PPhMe(Is))}$ (**6**), which decomposed even at low temperature to yield $\text{Pd}((R,R)\text{-Me-Duphos})_2$ and PPhMe(Is) (Scheme 4).^{6b}

(20) Data for minor diastereomer **5c** are included in Table 6 since these were reproducibly observed. In one sample of **5**, under conditions designed to maximize signal/noise, we also saw a minor (**5a/5d** ratio ca. 300:1) PMels peak due to another phosphido complex, **5d** (THF/THF-*d*₈, −70 °C, $\delta = -24.7$ (dd, $J = 117, 35$ Hz)). We could not detect the analogous Me-Duphos resonances or tell if this material was a diastereomer of **5a-c** or an impurity; this signal disappeared on warming. For more details on independent generation of the other potential impurities $\text{Pd}((R,R)\text{-Me-Duphos})(\text{Ph})(\text{PHIs})$ and $\text{Pd}((R,R)\text{-Me-Duphos})(\text{Me})(\text{PPhIs})$, see the Supporting Information.

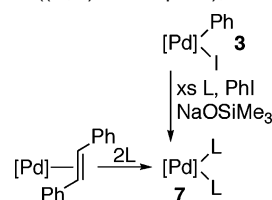
Scheme 5. $[\text{Pd}] = \text{Pd}((R,R)\text{-Me-Duphos})$, $\text{L} = \text{PHMe(Is)}$ 

Table S7 (Supporting Information) summarizes ^{31}P NMR data for **6** and analogous three-coordinate $\text{Pd}(\text{Duphos})$ complexes prepared in this study (see below).²¹

On decomposition of **5** in the presence of a trap (conditions more relevant to catalysis), three-coordinate complexes **6** were not observed. Warming a mixture of **5** and PhI gave phosphine **2** and oxidative addition product **3** (Scheme 4). These observations, along with kinetic studies of reductive elimination (see below), suggest that rate-determining formation of **6** from **5** was followed by rapid reaction with PhI to yield **3**. The $\text{Pd}(\text{Me-Duphos})$ fragment resulting from reductive elimination could also be trapped by the secondary phosphine substrate. During catalytic coupling of PHMe(Is) with PhI at room temperature, ^{31}P NMR monitoring initially showed the presence of phosphido complex **5** and $\text{Pd}((R,R)\text{-Me-Duphos})(\text{PHMe(Is)})_2$ (**7**), which underwent rapid exchange on the NMR time scale with PHMe(Is) . Complex **7** was generated free of **5** by running catalysis with a substoichiometric amount of PhI , or by addition of excess PHMe(Is) to $\text{Pd}((R,R)\text{-Me-Duphos})(\text{trans-stilbene})$ (Scheme 5). At −40 °C, phosphine exchange in **7** was slow on the NMR time scale and the expected mixture of four diastereomers was observed.

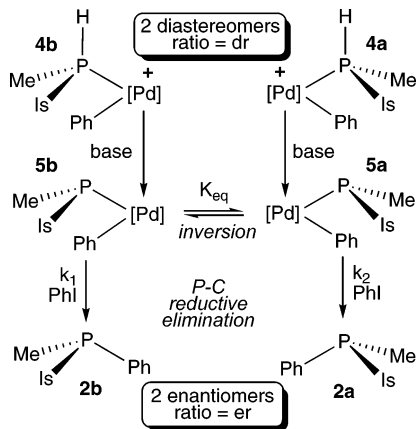
As catalysis proceeded, complex **3** was also observed; it became the dominant Pd species present near the end of the reaction. In catalysis with PhOTf , the same Pd complexes were observed,²² but the ratio of **7** to **5** was greater, consistent with faster oxidative addition of PhI .²³ These observations suggest that the rates of oxidative addition and reductive elimination during catalysis were similar and that Pd-P bond formation could be faster than both steps under appropriate conditions.

Scheme 6 shows how the relative rates of interconversion between invertomers *S_P*- and *R_P*-**5** and their reductive elimination might control enantioselection in catalysis. Note that this idealized scheme neglects possible contributions to product formation from diastereomer **5c** (or other rotamers), which were observed only at low temperature. Under catalytic conditions at room temperature, only one set of phosphido signals was observed; we cannot tell if this was an average resulting from coalescence of the **5a/5b** signals or if coalescence had not occurred, and peaks due to **5b** were too broadened to observe under these conditions.²⁴

If **5a** and **5b** both undergo reductive elimination faster than P inversion, then the enantiomeric ratio (er) of product **2** would

- (21) The simpler three-coordinate complexes $\text{Pd}((R,R)\text{-Me-Duphos})(\text{PR}_3)$ ($\text{R} = t\text{-Bu}$ or Cy) were prepared by reduction of $\text{Pd}((R,R)\text{-Me-Duphos})\text{Cl}_2$ with $\text{NaBH}(\text{OMe})_3$ in the presence of the ligand (see the Supporting Information for details). Although these complexes of bulky trialkylphosphines were more stable than **6**, they also decomposed to $\text{Pd}((R,R)\text{-Me-Duphos})_2$ at room temperature.
- (22) Reaction mixtures with PhOTf contained 1 equiv of NaI per Pd, derived from precursor **3**. Independent generation of $\text{Pd}((R,R)\text{-Me-Duphos})(\text{Ph})(\text{OTf})$ (from $\text{Pd}((R,R)\text{-Me-Duphos})(\text{trans-stilbene})$ and PhOTf) in the presence of NaI gave **3**, consistent with the observations in the catalytic system.
- (23) Alcazar-Roman, L. M.; Hartwig, J. F. *Organometallics* **2002**, *21*, 491–502.

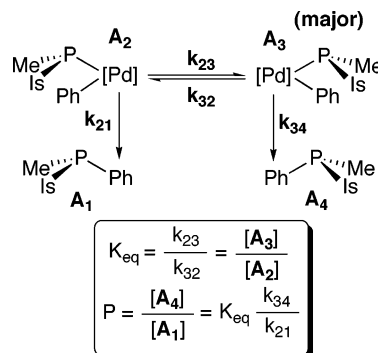
Scheme 6. Probing Relative Rates of P Inversion and Reductive Elimination in Phosphido Complex **5**: “er vs dr” Experiments ([Pd] = Pd((*R,R*)-Me-Duphos))



reflect the thermodynamic ratio of their precursors **4a** and **4b** (er = dr, Scheme 6). Alternatively, if interconversion of **5a** and **5b** is faster than reductive elimination, their relative abundance and reductive elimination rates might result in an er of **2** different from the original dr of cations **4** ($k_1 \neq k_2$; er \neq dr, Scheme 6).^{25–27} Deprotonation of 1:1 or 1.4:1 mixtures of cations **4-OTf** with NaOSiMe₃ in the presence of PhI gave phosphine **2** (er = 6:1).²⁸ Therefore, the rate of inversion was greater than or equal to that of reductive elimination under these conditions. Generating **5** by treatment of **3** with phosphine **1**, PhI, and NaOSiMe₃ at room temperature led to analogous results (er = 6:1).²⁸ The similar product ratio observed in the catalytic reactions provides a rationale for the observed enantioselection.²⁹

Mechanistic Hypothesis: Curtin–Hammett Kinetics. We hypothesized that inversion was *much faster* than reductive elimination in Scheme 6. Then, in an example of Curtin–Hammett kinetics, the product ratio $[2a]/[2b] = P = K_{eq}(k_{34}/k_{21})$ (Scheme 7; K_{eq} is the equilibrium constant for diastereomers **5a** and **5b**, while the rate constants describe their reductive elimination rates).²⁶ Note that Schemes 6 and 7 simplify the reductive elimination process by omitting the three-coordinate intermediate **6** (Scheme 4); this is justified because rate-determining formation of **6**, which fixes the P stereochemistry in the product **2**, is followed by fast release of the product. We

Scheme 7. Proposed Curtin–Hammett Kinetic Scheme for Inversion and Reductive Elimination in Phosphido Complex **5a**



^a [Pd] = Pd((*R,R*)-Me-Duphos). The labels for the compounds (**A1** and **A4** are phosphine **2**; **A2** and **A3** are phosphido complexes **5**) and the rate constants follow Seeman’s review.²⁶ Rate constants k_{23} and k_{32} describe the composite process of P inversion and rotation about the Pd–P bond which interconverts **A2** and **A3**, and rate constants k_{21} and k_{34} characterize reductive elimination of the phosphido diastereomers Pd((*R,R*)-Me-Duphos)(Ph)(PMeIs) (**A3** and **A2**, or **5a–b**). The *R_P* diastereomer **A3** is arbitrarily assumed to be the major one.

also assume that P–C reductive elimination proceeds with retention of configuration at P, as we showed earlier in reductive elimination of the analogous phosphido–borane complexes Pd–((*S,S*)-Chiraphos)(*o*-MeOC₆H₄)(PMePh(BH₃)).³⁰

Following Seeman’s review, the kinetics of such Curtin–Hammett systems can be described in terms of the empirical Winstein–Holness rate constant k_{WH} , which describes the total rate of product formation.²⁶

$$\frac{d}{dt}[A_1] + \frac{d}{dt}[A_4] = k_{WH}([A_2] + [A_3]) \quad (1)$$

After experimental measurement of k_{WH} , the reductive elimination rate constants k_{21} and k_{34} are given by

$$k_{34} = k_{WH} \left(\frac{K_{eq} + 1}{K_{eq}} \right) \left(\frac{P}{P + 1} \right) \quad (2)$$

$$k_{21} = k_{WH} \frac{(K_{eq} + 1)}{(P + 1)} \quad (3)$$

where K_{eq} and P are defined as in Scheme 7.

Kinetic Studies of Reductive Elimination from Phosphido Complex 5. Phosphido complex **5** was generated at -78°C in THF/THF-*d*₈ by deprotonation of cation **4-OTf** or by treatment of Pd((*R,R*)-Me-Duphos)(Ph)(I) (**3**) with PHMe(Is) and NaO-SiMe₃. In both cases, reductive elimination in the presence of PhI at -10°C gave PPhMe(Is) (**2**) and **3** (see Scheme 4); this process was observed by ³¹P NMR spectroscopy.

Since the two enantiomers of product **2** gave identical ³¹P NMR spectra, the Winstein–Holness rate constant k_{WH} could be measured directly by monitoring the growth of the phosphine over time by NMR spectroscopy. Alternatively, k_{WH} could be obtained by observing formation of Pd complex **3** or disappearance of the major phosphido diastereomer **5a** (we could not obtain reliable NMR integration for the broadened peaks of minor isomer **5b**). Both decomposition of **5a** and formation of the products fit first-order kinetics.³¹ Thus, concentration vs

- (24) Coalescence of the Pd–PMeIs ³¹P NMR signals near room temperature is plausible. Interconversion of **5a** and **5b** requires both P inversion and rotation about the Pd–P bond. An approximation for the barrier to this composite process at the coalescence temperature is $\Delta G^\ddagger_{TC} = 4.58T_c(10.32 + \log T_c/k_c)$ cal/mol, where $k_c = 2.22\Delta\nu$ (Friebolin, H. *Basic One- and Two-Dimensional NMR Spectroscopy*, 2nd ed.; VCH: Weinheim, Germany, 1993). Using the $\Delta\nu$ value from Table 6, measured at 202 MHz, coalescence at 298 K would correspond to a barrier of ca. 12 kcal/mol, similar to those for related Pt and Pd complexes.^{16,19}
- (25) Halpern, J. *Science* **1982**, *217*, 401–407.
- (26) Seeman, J. R. *Chem. Rev.* **1983**, *83*, 83–134. For an application in organometallic chemistry, see: Gately, D. A.; Norton, J. R. *J. Am. Chem. Soc.* **1996**, *118*, 3479–3489.
- (27) For a related experiment involving alkylation of Fe-phosphido complexes, see: Crisp, G. T.; Salem, G.; Wild, S. B.; Stephens, F. S. *Organometallics* **1989**, *8*, 2360–2367.
- (28) Small variations in er were observed; see the Supporting Information for results and estimation of the error in measurement of er.
- (29) Cations **4a** and **4b** might interconvert by dissociation of PHMe(Is), racemization of the phosphine by reversible deprotonation/protonation, and rebinding (Bader, A.; Nullmeyer, T.; Pabel, M.; Salem, G.; Willis, A. C.; Wild, S. B. *Inorg. Chem.* **1995**, *34*, 384–389). If this process occurred very quickly, and one of the diastereomeric cations was deprotonated more rapidly than the other, then it is possible that er \neq dr in Scheme 6, even if reductive elimination was faster than inversion. However, the lack of dependence of the ee in the catalytic reactions on the concentration or the nature of the base (Table 1, entries 11–14) suggests that the base, and, specifically, the deprotonation step, does not affect enantioselectivity.

- (30) (a) Moncarz, J. R.; Brunner, T. J.; Glueck, D. S.; Sommer, R. D.; Rheingold, A. L. *J. Am. Chem. Soc.* **2003**, *125*, 1180–1181. (b) Reference 6b.

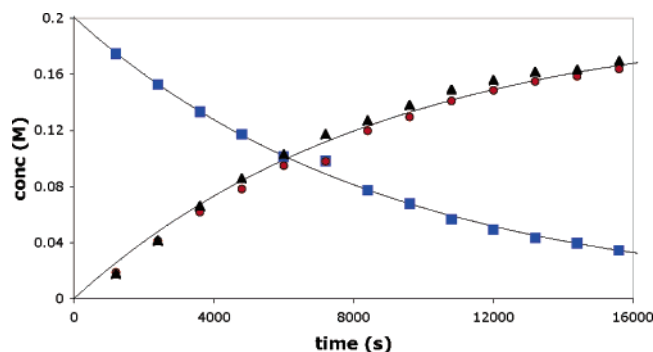


Figure 4. Concentration vs time plots for reductive elimination of **5** in the presence of PhI to yield **2** and **3** (THF/THF- d_8 , -10°C). Blue squares: [**5a**]. Red circles: [**2**]. Black triangles: [**3**]. The smooth lines are fits to the equations $A = A_0e^{-kt}$ and $B = A_0(1 - e^{-kt})$ for decay of **5a** (A) and growth of **2** and **3** (B) with $k = 1.13 \times 10^{-4} \text{ s}^{-1}$ ($r^2 = 0.996$ for decay of **5a**). The same value of k was used to fit the growth of products **2** and **3**. Directly fitting concentration vs time data for **2** and **3** yielded slightly different rate constants; see Table 7, entry 1 and the Supporting Information for more details.

time plots yielded three independent determinations of k_{WH} for each run (Figure 4; the smooth curves are fits to first-order decay of **5a** and growth of **2** (red circles) and **3** (black triangles)). As shown in Table 7, values for k_{WH} obtained by observing the disappearance of **5a** were consistent with those calculated from the appearance of the products **2** and **3**.

Decomposition of **5a** generally gave the most reliable fits; data for formation of products **2** and **3** are included in Table 7 as an indication of the error in determination of k_{WH} . The results did not differ significantly with the two different precursors (compare entries 1–4 and 5–6)³² or depend on initial concentration of **5**. Using higher concentrations of PhI gave similar results (Supporting Information), consistent with first-order decomposition.³³ Without PhI (entry 4), decomposition of **5** gave a mixture of diastereomers of three-coordinate intermediate **6**, which decomposed to yield **2**, Pd((*R,R*)-Me-Duphos)₂, and, presumably, Pd(0) (the ^{31}P NMR signal of **2** broadened over time, perhaps due to an exchange process with a zerovalent Pd complex of the phosphine). The first-order rate constant for decay of **5a** under these conditions was comparable to that in the presence of PhI. An approximate value for k_{WH} is then $1.5(\pm 0.5) \times 10^{-4} \text{ s}^{-1}$.

Extracting the reductive elimination rate constants k_{21} and k_{34} from eqs 2 and 3 required k_{WH} , the product ratio P , and K_{eq} . The kinetics studies yielded both k_{WH} and P . The latter was measured under conditions (see Table 7, entry 1 and the Supporting Information) where complete decomposition of **5** occurred at -10°C . Thus, the reaction was monitored until ca. 80% conversion. Samples were then transferred to a cold bath (-10°C , ice/brine/NaCl), which was placed in a freezer (-10°C) and stored for at least 24 h until the reaction was

complete. After isolation of the product phosphine, the ee (product ratio $P = 8:1$) was determined. Peak broadening and competing reductive elimination precluded similar direct measurement of K_{eq} at -10°C , but extrapolation of the data from Figure 3 gave $K_{\text{eq}} = 27$.

These results provided two kinetically indistinguishable sets of values for the reductive elimination rate constants k_{21} and k_{34} of Scheme 7. If the major product phosphine was formed from the major starting material (case 1, $K_{\text{eq}} = 27$, $P = 8$), $k_{34} = 1.4 \times 10^{-4} \text{ s}^{-1}$ and $k_{21} = 4.7 \times 10^{-4} \text{ s}^{-1}$.³⁴ Alternatively, if the minor starting material yielded the major product (case 2, $K_{\text{eq}} = 27$, $P = 1/8$), then $k_{34} = 1.7 \times 10^{-5} \text{ s}^{-1}$ and $k_{21} = 3.7 \times 10^{-3} \text{ s}^{-1}$.³⁴ Thus, in both cases, reductive elimination of the minor phosphido intermediate **5b** occurred more quickly than that for the major one. If **5b** decayed about 3 times faster than **5a** (case 1), this would simply reduce the ee, which would still be controlled by the thermodynamic preference for **5a**. In case 2, however, where reductive elimination of **5b** is about 200 times faster than that of **5a**, the effect of K_{eq} on the product ratio would be outweighed by the relative rates of reductive elimination.

These results enabled us to confirm the hypothesis that P inversion in phosphido intermediates **5** was much faster than reductive elimination (Schemes 6 and 7). We have shown previously that the barrier to P inversion in analogous Pt and Pd phosphido complexes was the same within experimental error.^{19c} It was not possible to measure the rate of P inversion in **5**. However, the rate constants for the process of inversion and rotation about the Pt–P bond which interconverts the diastereomers of the Pt analogues Pt((*R,R*)-*i*-Pr-Duphos)(Ph)(PMeIs) (**8-Pt**) and Pt((*R,R*)-Me-Duphos)(I)(PMeIs) were ca. $5 \times 10^2 \text{ s}^{-1}$ and $8 \times 10^2 \text{ s}^{-1}$ at the coalescence temperature of -10°C ,²⁴ respectively, at least 10^5 times greater than the rate constants for reductive elimination from **5** at the same temperature.^{16b}

Absolute Configurations of the Products and Intermediates. Determination of the absolute configurations of the product phosphine **2** and the intermediate phosphido complexes **5** would distinguish the two possibilities described above and thereby establish the origin of enantioselectivity in the catalytic asymmetric synthesis of **2** from **1**.

A suitable phosphine, P(*p*-MeOC₆H₄)Me(Is) (**2-An**), was prepared catalytically in 83% ee. As discussed above, the consistent trends in the ^{31}P and ^1H NMR spectra of the adducts of the phosphines in Table 3 with Pd((*S*)-Me₂NCH(Me)C₆H₄)(μ -Cl)₂ suggested that the major enantiomer of this phosphine and its Ph analogue **2** had the same absolute configuration (see the Supporting Information). Six recrystallizations of **2-An** from *i*-PrOH gave a white crystalline solid with ee >99% by HPLC on a chiral stationary phase (ChiralPak AD; see the Supporting Information for details). The crystal structure of this highly enriched sample showed the presence of two independent molecules per asymmetric unit. Both had *S_P*-configuration (Figure 5). Chiral HPLC analysis of the single crystal used for structure determination confirmed that it was the major enan-

(31) (a) See the Supporting Information for demonstration that k_{WH} can be measured by observing decay of either diastereomer of starting material **5**, as a complement to the more usual method, observing product formation. (b) Concentration vs time data were fit using TableCurve2D software (SYSTAT Software Inc., <http://www.systat.com/products/TableCurve2D/help/?sec=1106>, accessed July 2006), using $A = A_0e^{-kt}$ and $[B] = [A_0](1 - e^{-kt})$ respectively for the first-order formation of B from A. See the Supporting Information for more details.

(32) The different precursors yielded **5** along with the byproducts NaOTf and NaI, respectively. While it is possible that the presence of these salts might lead to different rates of reductive elimination, our data are indistinguishable within experimental error.

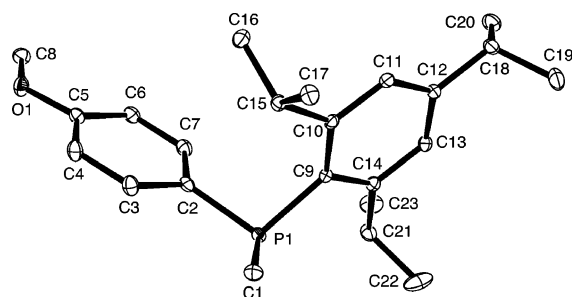
(33) Hartwig, J. F. *Acc. Chem. Res.* **1998**, *31*, 852–860.

(34) The error in determining k_{WH} is relatively large (Table 7), while there are also errors associated with the measurement of K_{eq} and P and, hence, the derived rate constants k_{21} and k_{34} . For our purposes of comparing the magnitude of k_{21}/k_{34} with k_{23}/k_{32} and determining which diastereomer of **5** leads to the major product, however, it is not necessary to determine these numbers with great precision.

Table 7. Kinetics Data for Reductive Elimination from Pd((*R,R*)-Me-Duphos)(Ph)(PMels) (**5**) in the Presence of PhI at $-10\text{ }^{\circ}\text{C}$ in THF/THF- d_8 ^a

entry	precursor	equiv of PhI	$k_{\text{WH}} (\text{s}^{-1})$, decay of 5a	$k_{\text{WH}} (\text{s}^{-1})$, formation of 2	$k_{\text{WH}} (\text{s}^{-1})$, formation of 3	$k_{\text{WH}} (\text{s}^{-1})$, average
1 ^b	A (0.20 M)	2	1.13×10^{-4}	9.06×10^{-5}	1.07×10^{-4}	1.04×10^{-4}
2	A (0.187 M)	1.5	1.31×10^{-4}	8.60×10^{-5}	^c	1.09×10^{-4}
3	A (0.11 M)	1.9	1.34×10^{-4}	2.12×10^{-4}	2.63×10^{-4}	2.03×10^{-4}
4	A (0.15 M)	0	1.92×10^{-4}	^d	^d	1.92×10^{-4}
5	B (0.145 M)	2	1.28×10^{-4}	1.19×10^{-4}	9.19×10^{-5}	1.13×10^{-4}
6	B (0.20 M)	2	1.49×10^{-4}	2.33×10^{-4}	1.94×10^{-4}	1.92×10^{-4}

^a Phosphido complex **5** was generated by deprotonation of precursor **A** (**4-OTf**) with NaOSiMe₃ or by treatment of precursor **B** (**3**) with PHMe(Is) and NaOSiMe₃. As in Figure 4, concentration vs time data for **5a**, **2**, and **3** were fit separately to first-order exponential functions. See Experimental Section and Supporting Information for more details. ^bProduct ee = 79%. ^cConcentration vs time data for **3** were too noisy to give an acceptable fit. ^dWithout the PhI trap, **3** was not formed, and formation and decomposition of the intermediate **6** prevented monitoring [**2**] over time.

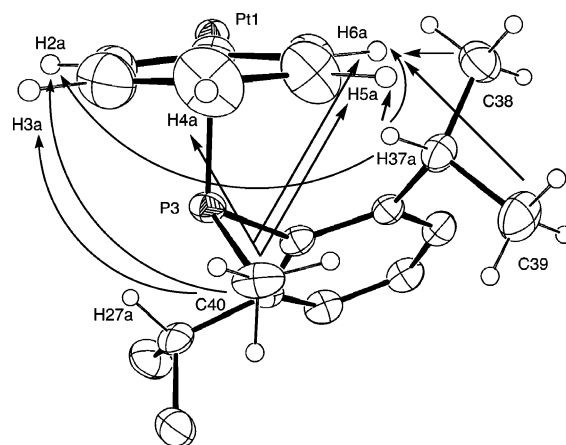
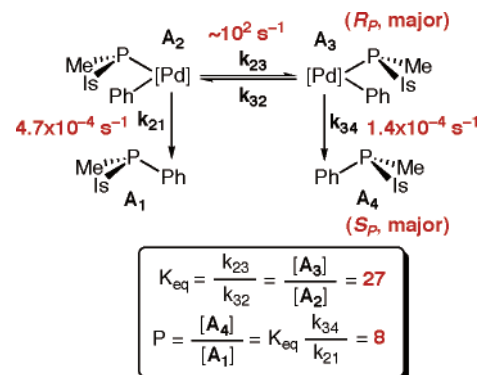
**Figure 5.** ORTEP diagram of one of the two independent molecules of *S_P*-P(*p*-MeOC₆H₄)Me(Is) (**2-An**).

tiomer of phosphine **2-An**. Racemic **2-An** crystallized in a different space group (Supporting Information).

We could not crystallize thermally unstable intermediate **5**, so its absolute configuration was investigated by low-temperature NMR spectroscopy, with comparison to NMR and crystallographic results for *R_P*-**5-Pt**.^{16b,18} The similarity between the structures of cations **4** and **4-Pt** (Table 5) suggested that **5-Pt** would be a good structural model for **5**. Unfortunately, direct confirmation that the solution structure of the major diastereomer of **5-Pt** was the same as that in the solid state was not possible because rapid P inversion would interconvert the diastereomers even at low temperature. However, low-temperature NOESY studies of **5-Pt** showed that the solution structure of the major diastereomer was consistent with the solid-state one (*R_P*).¹⁸ In the absence of similar NMR data for the minor isomer, not available because of its low concentration, we could not rule out the possibility that the major solution isomer is actually *S_P*. However, comparison to the structures of Pt(*R,R*)-*i*-Pr-Duphos)(Ph)(PMels) (**8-Pt**) and related complexes described elsewhere suggested that the major diastereomer of **5-Pt** contained an *R_P* phosphido group.¹⁸

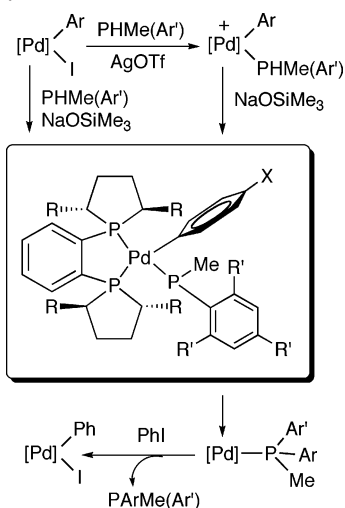
Multinuclear NMR and NOESY data for the major diastereomers of **5** and **5-Pt** were in excellent agreement (Supporting Information), so it is likely that the absolute configuration of major diastereomer **5a** was also *R_P*. Figure 6 shows selected NOEs between PMels and Pd–Ph hydrogens in **5a**, which are consistent with the solid-state structure of **5-Pt** (see the footnote in Figure 6 for selected H–H distances, estimated using the calculated hydrogen atom positions, which correspond to the observed NOEs).

Since P–C reductive elimination from Pd(II) proceeded with retention of configuration, *S_P*-**2** must be formed from *R_P*-**5**.³⁰ (The apparent inversion of configuration is a consequence of the sequence rules as a P–Pd bond is converted to a P–Ph bond.) Thus, it appears that the major enantiomer of product

**Figure 6.** Partial ORTEP diagram of **5-Pt**,^{16b} used as a model to show NOEs observed between Pd–Ph hydrogens H2–H6 and the PMels hydrogens (C40 = P–Me; C38 and C39 = *i*-Pr Me; H37 = *i*-Pr CH) in the major diastereomer **5a** (THF/THF- d_8 , $-50\text{ }^{\circ}\text{C}$). Selected distances in **5-Pt** (in Å) were estimated using the calculated hydrogen atom positions: H37–H6 2.393, H37–H5 4.495, H37–H2 4.895, H38–H6 3.860 (av), H39–H6 3.790 (av), H40–H2 4.099 (av), H40–H3 4.851 (av), H40–H4 5.053 (av), H40–H5 4.400 (av), H40–H6 3.532 (av).**Scheme 8.** Approximate Rate and Equilibrium Constants for Inversion and Reductive Elimination of **5a** (**A₃**) and **5b** (**A₂**) at $-10\text{ }^{\circ}\text{C}$ in THF ([Pd] = Pd((*R,R*)-Me-Duphos))

phosphine **2** was formed from the major diastereomer of intermediate phosphido complex **5**. Scheme 8 summarizes these conclusions and includes the approximate reductive elimination and inversion rate constants.

In contrast to the classic major-product-from-minor-intermediate result in asymmetric hydrogenation,^{25,35} these results suggest that enantioselectivity was determined mainly by the thermodynamic preference for **5a**, although faster reductive elimination of minor diastereomer **5b** reduced the product ratio. We reached a similar conclusion in Pt-catalyzed asymmetric

Scheme 9. Structure–Reactivity Relationships in Pd(Duphos) Aryl Phosphido Complexes^a

^a Phosphido complexes: [Pd] = Pd((*R,R*)-*i*-Pr-Duphos) (R = *i*-Pr), X = H, R' = *i*-Pr (**8**); [Pd] = Pd((*R,R*)-Me-Duphos) (R = Me), X = H, R' = *i*-Pr (**5**), R' = Ph (**9**), R' = Me (**10**); R' = *i*-Pr, X = NH₂ (**5-NH₂**), X = I (**5-I**), X = NO₂ (**5-NO₂**).

alkylation involving the closely related intermediate **5-Pt**, where P–C bond formation involved nucleophilic attack of the phosphido group on benzyl bromide.¹⁸

Structure–Reactivity Relationships. Assuming that this mechanistic model is a general one, we generated a series of derivatives Pd(diphos*)(Ar)(PMeAr') to investigate the dependence of dr (K_{eq}), reductive elimination rate, and ee on the Pd-bound chiral diphosphine ligand, the secondary phosphine substrate, and the aryl iodide (Scheme 9). The intermediates were formed either on direct treatment of Pd(diphos*)(Ar)(I) with PHMe(Ar') and NaOSiMe₃ or on deprotonation of the cations [Pd(diphos*)(Ar)(PHMe(Ar'))][OTf]. ³¹P NMR data for these phosphido complexes (Supporting Information) were similar to those shown in Table 6 for **5**.

Diphos*. Pd((*R,R*)-*i*-Pr-Duphos)(Ph)(PMeIs) (**8**), as observed for **8-Pt**, existed as a mixture of four diastereomers at low temperature.¹⁶ We presume that each of the expected “invertomers,” which differ in their phosphido P configuration, was a mixture of two rotamers in these sterically hindered complexes. Changing from Me-Duphos in **5** to *i*-Pr-Duphos in **8** (and in the Pt analogues) reduced the diastereomeric ratio (Table 8) and also affected the kinetics of reductive elimination. P–C bond formation in **8** occurred even at –60 °C, under conditions where **5** decomposed very slowly. Apparently, a combination of these factors resulted in the unusual observation that these ligands, of opposite absolute configuration, gave the same enantiomer of **2** with very similar ee in catalysis (Table 2).¹⁰ These results were consistent with the models of Schemes 7 and 8, but a similar quantitative analysis was not possible because of the presence of appreciable quantities of three diastereomers of **8** at low temperature.

Phosphido Ligand. The dr was also strongly affected by modifying the P–aryl substituent (Table 8). Only one diaste-

Table 8. Substituent Effects on Diastereomer Ratio in the Phosphido Complexes Pd((*R,R*)-Duphos)(Ph)(PMeAr') at –60 °C in THF^a

Duphos (number)	Ar'	dr
(<i>R,R</i>)- <i>i</i> -Pr-Duphos (8)	Is	31:1:4:3
(<i>R,R</i>)-Me-Duphos (5)	Is	137:2.4:1
(<i>R,R</i>)-Me-Duphos (9)	Phes	>100:1 ^b
(<i>R,R</i>)-Me-Duphos (10)	Mes	7.3:1

^a Diastereomer ratios were determined by ³¹P NMR integration. Four diastereomers were observed for **8**, three for **5**,²⁰ only one for **9**, and two for **10**. ^bOnly one diastereomer of **9** was observed.

Table 9. Substituent Effects on Diastereomer Ratio (K_{eq}) in the Phosphido Complexes Pd((*R,R*)-Me-Duphos)(*p*-XC₆H₄)(PMeIs) at –60 °C in THF^a

X	K_{eq}	σ_p^{12}
NH ₂	34	–0.32
MeO	48	–0.27
H	57	0
I	33	0.18
NO ₂	56	0.78

^a The equilibrium constants (diastereomer ratios between **5a** and **5b** and their analogues) were determined by ³¹P NMR integration.

reomer of Pd((*R,R*)-Me-Duphos)(Ph)(PMePhes) (**9**) was observed; the dr at –60 °C was lower for PMeIs analogue **5** (three diastereomers) and lower still for the two diastereomers of PMeMes complex **10**, as expected if the equilibrium constant depended strongly on steric effects. Reductive elimination from PMePhes complex **9**, which occurred at –60 °C, was faster than that in **5**. So was decomposition of PMeMes complex **10**, which took about 3 h at –20 °C (compare **5**, in which reductive elimination was not complete after 3 h at –10 °C). Decomposition of Pd((*R,R*)-Me-Duphos)(Ph)(PMePhes) (**9**) in the presence of PhI gave a mixture of the three-coordinate Pd((*R,R*)-Me-Duphos)(Ph)(PPhMe(Phes)) (**6-Phes**) and **3**, which suggests that, in contrast to **5**, reductive elimination and trapping of Pd(0) with PhI were similar in rate. Thus, modifying the aryl substituent in the phosphido ligand resulted in significant changes to both thermodynamics and kinetics of these analogues of **5**. However, generation and reductive elimination of **9** and **10**, at least in our initial experiments, was less clean than the chemistry of **5**, precluding analogous kinetic studies of reductive elimination.

Pd–Ar Group. We generated a series of Pd((*R,R*)-Me-Duphos)(*p*-XC₆H₄)(PMeIs) intermediates (X = NH₂, MeO, H, I, NO₂) to assess the effect of the *para* substituent on the equilibrium between the diastereomers and their rates of reductive elimination. Table 9 shows the dependence of K_{eq} ([**5a**]/[**5b**], as in Figure 3) at –60 °C on the aryl substituent. As expected, given the evidence above for steric effects on diastereomer ratio, the values were large and similar in magnitude. The variations observed at this temperature did not correlate with the electronic properties of the *p*-substituents as judged by their Hammett constants or with enantioselectivity in catalysis (Table 3, Figure 1).

Reductive elimination rates were qualitatively similar in this series, except for the *p*-NO₂ derivative, which underwent anomalously fast reductive elimination, even at –70 °C. In the crystal structure of Pd((*R,R*)-Me-Duphos)(*p*-NO₂C₆H₄)(I) (Supporting Information), the Pd–C bond length of 2.060(4) Å (average value, two molecules in the unit cell) was slightly shorter than that in the Pd–Ph derivative (2.084(3) Å).⁹ Thus,

(35) (a) Landis, C. R.; Halpern, J. *J. Am. Chem. Soc.* **1987**, *109*, 1746–1754. (b) Drexler, H.-J.; Baumann, W.; Schmidt, T.; Zhang, S.; Sun, A.; Spannenberg, A.; Fischer, C.; Buschmann, H.; Heller, D. *Angew. Chem., Int. Ed.* **2005**, *44*, 1184–1188. (c) Schmidt, T.; Baumann, W.; Drexler, H.-J.; Arrieta, A.; Heller, D.; Buschmann, H. *Organometallics* **2005**, *24*, 3842–3848.

it seems unlikely that a ground-state effect based on large changes in the Pd–C bond strength could explain the relative rates of reductive elimination. Instead, a transition-state effect based on the increased electrophilicity of the Ar group may explain this observation and, more generally, the fast reductive elimination for *p*-nitrophenyl groups in Pd-mediated formation of C–X bonds (X = N, O, S, P).^{33,36}

Thus, changes in the structure of the key intermediate Pd-(Duphos)(Ar)(PMeAr') had significant effects on both the equilibrium between the diastereomers and the rate of reductive elimination. The lack of correlation between dr, reductive elimination rate, and enantioselectivity in catalysis (Table 3) is consistent with the CHWH model for enantioselection (Scheme 7).

Conclusions

We have described enantioselective synthesis of P-stereogenic phosphines by Pd-catalyzed asymmetric phosphination. The reaction proceeded in high yields and up to 88% ee. Several chiral diphosphines were suitable ligands; Me-Duphos resulted in the highest selectivity for the test cross-coupling of PHMe(Is) and PhI. A variety of aryl iodides and secondary phosphines could be used; enantioselectivity depended strongly on substrate structure. Sterically demanding secondary phosphine Ar' substituents and aryl iodides with electron-donating para substituents gave the highest ee values.

Kinetic studies of reductive elimination suggested that the rate of phosphorus inversion in the diastereomeric Pd-phosphido intermediates Pd((*R,R*)-Me-Duphos)(Ph)(PMeIs) (**5**) was much faster than the rate of subsequent reductive elimination. As a result of this Curtin–Hammett behavior, summarized in Schemes 7 and 8, the product ratio depended on both the equilibrium ratio of diastereomers **5** and their relative rates of reductive elimination ($P = K_{eq}(k_{34}/k_{21})$).

The substituent effects observed highlight the problems and opportunities this mode of enantioselection poses for rational catalyst design. From both this work and analogous Pt chemistry, it appears relatively easy to engineer phosphido intermediates with a large K_{eq} by using phosphido substituents of markedly different size.¹⁶ The hard part, which remains a general challenge in asymmetric catalysis, is to control the relative rates of reaction of major and minor diastereomers (k_{34}/k_{21}). In the case of **5**, studied in detail here, the faster reductive elimination of the minor diastereomer ($k_{34}/k_{21} \approx 1/3$) worked against K_{eq} to result in a reduced ee. Further studies in these and related systems will seek to understand the factors which control this reactivity, in order to design systems where the major diastereomer reacts more quickly than the minor one.

Experimental Section

General Details. Unless otherwise noted, all reactions and manipulations were performed in dry glassware under a nitrogen atmosphere at 20 °C in a dry box or using standard Schlenk techniques. Petroleum ether (bp 38–53 °C), ether, THF, CH₂Cl₂, and toluene were dried using activated alumina columns similar to those described by Grubbs.³⁷ NMR spectra were recorded by using Varian 300 or 500 MHz spectrometers.

(36) Widenhoefer, R. A.; Buchwald, S. L. *J. Am. Chem. Soc.* **1998**, *120*, 6504–6511.

(37) Pangborn, A. B.; Giardello, M. A.; Grubbs, R. H.; Rosen, R. K.; Timmers, F. J. *Organometallics* **1996**, *15*, 1518–1520.

¹H or ¹³C NMR chemical shifts are reported vs Me₄Si and were determined by reference to the residual ¹H or ¹³C solvent peaks. ³¹P NMR chemical shifts are reported vs H₃PO₄ (85%) used as an external reference. Coupling constants are reported in Hz. Unless otherwise noted, peaks in NMR spectra are singlets, and absolute values are reported for coupling constants. Elemental analyses were provided by the Schwarzkopf Microanalytical Laboratory. Mass spectra were obtained at the University of Illinois Urbana–Champaign.

Unless otherwise noted, reagents were from commercial suppliers. The following compounds were prepared by literature procedures: 8-iodoquinoline,³⁸ (*N,N*)-dimethyl-4-iodo-aniline,³⁹ FeI (Fc = C₅H₅–FeC₅H₄),⁴⁰ CymI (Cym = C₅H₄Mn(CO)₃),⁴¹ PHMe(Is) and PHMe(Mes*),⁸ (Pd(*S*)-Me₂NCH(Me)C₆H₄)(μ-Cl))₂,⁴² Pd(diphos*)(*trans*-stilbene), Pd((*R,R*)-Me-Duphos)(Ph)(I) and Pd(Me-FerrolANE)(Ph)(I),⁹ PhesBr,⁴³ Pd(*p*-Tol)₃Cl₂,⁴⁴ and Pd(TMEDA)(*p*-NO₂C₆H₄)(I).⁴⁵ Syntheses of the secondary phosphines PHMe(Phes) and PHMe(Mes) are described in the Supporting Information.

General Procedure for Catalysis. To a solution of Pd((*R,R*)-Me-Duphos)(Ph)(I) (3 mg, 0.004 mmol, 0.05 equiv) in toluene (0.5 mL) in a 20 mL vial was added PhI (11 μL, 0.092 mmol), followed by PHMe(Is) (23 mg, 0.092 mmol) and then NaOSiMe₃ (92 μL of a 1.0 M THF solution, 0.092 mmol). The pale yellow solution turned dark yellow and then orange upon addition of the base. The solution was transferred to an NMR tube, and the vial was rinsed with additional toluene (0.5 mL), which was then transferred to the NMR tube. After ca. 10 min a white solid precipitated. The progress of the reaction was monitored by ³¹P{¹H} NMR. Once the reaction was complete (ca. 1 h), the solvent was removed *in vacuo*. The yellow residue was dissolved in THF (0.5 mL), and the product phosphine was purified by column chromatography on silica (9:1 petroleum ether/THF eluent, 4 in. column, 1 cm diameter) and isolated as a clear colorless oil which became a white solid upon storage at –25 °C for 4 d to give 16 mg (53% yield) of isolated product. See the Supporting Information for ee and NMR yield determination.

[Pd((*R,R*)-Me-Duphos)(Ph)(PHMe(Is))][OTf] (4a–b**).** To a stirring solution of Pd((*R,R*)-Me-Duphos)(Ph)(I) (75 mg, 0.12 mmol) in THF (2 mL) was added PHMe(Is) (31 mg, 0.12 mmol) followed by dropwise addition of AgOTf (32 mg, 0.12 mmol), giving a brown precipitate. The reaction mixture was stirred for 30 min. The solution was filtered through Celite. The precipitate was rinsed with THF (2 × 2 mL). The yellow-greenish solution was concentrated *in vacuo*. The ³¹P{¹H} NMR spectrum showed a 1:1 ratio of diastereomers. The solution was layered with petroleum ether and cooled overnight at –25 °C to yield a yellow oil. Trituration with petroleum ether gave a pale-yellow solid, which was dried *in vacuo* to yield 81 mg (75%) of product as a 1:1 mixture of diastereomers.

Anal. Calcd for C₄₁H₆₀F₃O₃P₃PdS: C, 55.38; H, 6.80. Found: C, 55.44; H, 6.75. ³¹P{¹H} NMR (THF-*d*₈), **a** and **b** are the two diastereomers: δ 73.5 (dd, *J* = 24, 26, **a**), 72.0 (dd, *J* = 369, 24, **b**), 70.4 (dd, *J* = 29, 24, **b**), 69.8 (dd, *J* = 375, 26, **a**), –54.3 (br dd, *J* = 375, 24, **a**), –59.0 (dd, *J* = 369, 29, **b**). ¹H NMR (THF-*d*₈): δ 8.17–8.14 (m, 1H, Ar), 8.08–8.00 (m, 3H, Ar), 7.86–7.78 (m, 4H, Ar), 7.72–7.70 (m, 1H, Ar), 7.42–7.40 (m, 1H, Ar), 7.38–7.35 (m, 1H, Ar), 7.27–7.20 (m, 5H, Ar), 7.16–7.11 (m, 2H, Ar), 7.08–7.05 (m, 1H, Ar), 6.98–6.97 (m, 1H, Ar), 6.94–6.91 (m, 1H, Ar), 6.75–6.72 (m, 1H, Ar), 6.63 (dm, *J*_{PH} = 355, 1H, PH), 6.32 (dm, *J*_{PH} = 373, 1H,

(38) Kondo, Y.; Manabu, S.; Uchiyama, M.; Sakamoto, T. *J. Am. Chem. Soc.* **1999**, *121*, 3539–3540.

(39) Barluenga, J.; Gonzalez, J. M.; Garcia-Martin, M. A.; Campos, P. J.; Asensio, G. *J. Org. Chem.* **1993**, *58*, 2058–2060.

(40) Guilleaux, D.; Kagan, H. B. *J. Org. Chem.* **1995**, *60*, 2502–2505.

(41) Lo Sterzo, C.; Miller, M. M.; Stille, J. K. *Organometallics* **1989**, *8*, 2331–2337.

(42) Tani, K.; Brown, L. D.; Ahmed, J.; Ibers, J. A.; Nakamura, A.; Otsuka, S.; Yokota, M. *J. Am. Chem. Soc.* **1977**, *99*, 7876–7886.

(43) Olmstead, M. M.; Power, P. P. *J. Organomet. Chem.* **1991**, *408*, 1–6.

(44) Paul, F.; Patt, J.; Hartwig, J. F. *Organometallics* **1995**, *14*, 3030–3039.

(45) Kruis, D.; Markies, B. A.; Cauty, A. J.; Boersma, J.; van Koten, G. J. *Organomet. Chem.* **1997**, *532*, 235–242.

PH), 3.78–3.71 (m, 2H), 3.28–2.80 (m, 10H), 2.62–2.12 (m, 6H), 2.03–1.79 (m, 6H), 1.71–1.56 (m, 3H), 1.71–1.67 (m, 3H, P–Me, overlapping with previous signals), 1.53 (dd, $J_{\text{PH}} = 7$, $J_{\text{HH}} = 4$, 3H, Me), 1.49 (dd, $J_{\text{PH}} = 7$, $J_{\text{HH}} = 3$, 3H, Me), 1.38 (d, $J_{\text{HH}} = 6$, 6H, *i*-Pr), 1.33 (d, $J_{\text{HH}} = 6$, 6H, *i*-Pr), 1.29 (d, $J_{\text{HH}} = 7$, 6H, *i*-Pr), 1.27 (d, $J_{\text{HH}} = 6$, 6H, *i*-Pr), 1.26 (d, $J_{\text{HH}} = 7$, 6H, *i*-Pr), 1.39–1.25 (m, 2H, overlapping with previous signals), 1.17 (dd, $J_{\text{PH}} = 15$, $J_{\text{HH}} = 7$, 3H, Me), 1.21–1.13 (m, 7H, overlapping with previous signals), 1.06–1.02 (m, 3H, P–Me), 0.93–0.82 (m, 9H), 0.83 (dd, $J_{\text{PH}} = 14$, $J_{\text{HH}} = 7$, 3H, Me, overlapping with previous peak), 0.75 (dd, $J_{\text{PH}} = 15$, $J_{\text{HH}} = 7$, 3H, Me). IR (KBr): 2960, 2918, 2863, 1650, 1634, 1562, 1458, 1419, 1381, 1271, 1221, 1145, 1117, 1023, 897, 765, 734, 699, 638, 528, 451.

Changing the Diastereomeric Ratio of Cations 4. Method I. A solution of **4-OTf** (30 mg, 0.034 mmol) in THF with initial diastereomeric ratio 1:1 was heated at 50 °C for 46 h. The diastereomeric ratio changed to 1:1.4 (a/b). **Method II.** To a stirred solution of Pd((*R,R*)-Me-Duphos)(Ph)(I) (50 mg, 0.081 mmol) in THF (2 mL) was added PHMe(Is) (40.6 mg, 0.162 mmol, 2 equiv). After 5 min, when the reaction mixture changed color from pale yellow to orange-brown, AgOTf (22.5 mg, 0.087 mmol, 1.1 equiv) was added as a suspension in THF (2 mL); a gray-brown precipitate formed. The reaction mixture was filtered and concentrated to 0.5 mL. Petroleum ether was layered on top of the solution, and slow diffusion overnight in a refrigerator yielded a brown oil that solidified upon trituration with petroleum ether. The diastereomeric ratio of the resulting compound was 1:1.4 (a/b).

Generation of Pd((*R,R*)-Me-Duphos)(Ph)(PMeIs) (5a–b). Method 1. To a cold (–78 °C) solution of Pd((*R,R*)-Me-Duphos)(Ph)(I) (**3**, 45 mg, 0.07 mmol), PHMe(Is) (18 mg, 0.07 mmol), and PhI (9 μL , 0.08 mmol, 1.1 equiv) in THF/THF- d_8 (1.5 mL, 1:1) in an NMR tube was added NaOSiMe₃ (73 μL of a 1.0 M solution in THF, 0.073 mmol). The tube was placed in the precooled (–50 °C) NMR probe. **Method 2.** To a cold (–78 °C) solution of **4-OTf** (generated *in situ* by reaction of Pd((*R,R*)-Me-Duphos)(Ph)(I) (44 mg, 0.07 mmol), PHMe(Is) (18 mg, 0.07 mmol), and AgOTf (18 mg, 0.07 mmol) in the presence of PhI followed by filtration to remove AgI; alternatively, isolated **4-OTf** was used) was added NaOSiMe₃ (71 μL of a 1.0 M solution in THF, 0.071 mmol). The tube was placed in the precooled (–50 °C) NMR probe. In both cases, a color change to orange was observed on formation of **5**.

³¹P NMR Study of Catalysis at Room Temperature. An NMR tube equipped with a rubber septum was charged with Pd((*R,R*)-Me-Duphos)(Ph)(I) (21 mg, 0.034 mmol), PHMe(Is) (85 mg, 0.34 mmol, 10 equiv), and PhI (71 mg, 0.35 mmol, 10.2 equiv) in ca. 1 mL of THF with a few drops of THF- d_8 added. The tube was cooled to –78 °C, and NaOSiMe₃ (350 μL of 1.0 M solution in THF, 0.35 mmol, 10.3 equiv) was added via cannula. The tube was briefly inverted in the cold bath to mix it and then placed in the NMR probe at 21 °C. The reaction was monitored by ³¹P NMR over ca. 1 h, when it was complete. A related experiment was done on the same scale, but using PhOTf (79 mg, 0.35 mmol) instead of PhI.

Deprotonation of Cations 4a–b (er vs dr Experiments). To a solution of Pd((*R,R*)-Me-Duphos)(Ph)(I) (**3**, 29 mg, 0.047 mmol) in THF (1 mL) were added PHMe(Is) (12 mg, 0.047 mmol) and PhI (10 μL , 0.089 mmol, 1.9 equiv). This reaction mixture was added to solid AgOTf (12 mg, 0.047 mmol). A white solid precipitated, and the mixture was filtered through Celite twice and then transferred into an NMR tube fitted with a rubber septum. ³¹P{¹H} NMR (THF) of this mixture showed a 1:1 ratio of cations **4a** and **4b**. NaOSiMe₃ (48 μL of a 1.0 M THF solution, 0.048 mmol) was added via microliter syringe, and the mixture immediately turned orange. The reaction was complete (by ³¹P{¹H} NMR) after 1 h, and black solid was observed in the NMR tube. The reaction mixture was filtered through Celite, and the solvent was removed *in vacuo*. Isolation, purification, and ee determination of **2** were performed as described above. Similar experiments were also done on isolated samples of **4-OTf** having different diastereomer ratios (1:1 and 1.4:1). See the Supporting Information for details.

Sample Procedure for Kinetics Experiments: Reductive Elimination from Pd–Phosphido Intermediates in the Presence of PhI.

Method I. To a solution of **4-OTf** (53.4 mg, 0.06 mmol) in 1 mL of THF/THF- d_8 was added PhI (7 μL , 0.06 mmol, 1 equiv) via syringe. The reaction mixture was transferred to the inner part of a coaxial NMR tube, which contained PPh₂Me (~5 mg) in 0.2 mL of THF in the outer part of the tube as an external standard. The tube was capped with a septum and cooled to –78 °C. NaOSiMe₃ (60 μL , 1.0 M solution in THF, 0.06 mmol) was injected via syringe, and the tube was transferred to the precooled NMR probe. The reaction was monitored by ³¹P{¹H} NMR spectroscopy until ca. 80% reaction completion. Then the NMR tube was transferred to a –10 °C cold bath (ice/brine/NaCl) and kept in a –10 °C refrigerator for 24 h. Isolation of the product and determination of the ee were done according to the standard procedure.

Method II. To a solution of **3** (49.3 mg, 0.08 mmol) was added PhI (18 μL , 33 mg, 0.16 mmol, 2 equiv) via syringe followed by PHMe(Is) (20 mg, 0.08 mmol) as a solution in 0.5 mL of THF with several drops of THF- d_8 . The reaction mixture was transferred to the inner part of a coaxial NMR tube as described above. The tube was capped with a septum and cooled to –78 °C. NaOSiMe₃ (80 μL , 1.0 M solution in THF, 0.08 mmol) was injected via syringe, and the tube was transferred to the precooled (–10 °C) NMR probe. Reaction monitoring and workup were as those in Method I above.

Acknowledgment. We thank the National Science Foundation, Union Carbide (Innovation Recognition Program), and the Beckman Foundation (Scholarship for O.A.) for support, and Solvias and Eastman for gifts of chiral phosphines.

Supporting Information Available: Experimental procedures and characterization data. This material is available free of charge via the Internet at <http://pubs.acs.org>.

JA070225A